The 2017 World Congress on
Advances in Structural Engineering and Mechanics (ASEM17)
28 August - 1 September, 2017, Ilsan(Seoul), Korea

Keynote Paper

Buckling Restrained Braces for Existing and New Reinforced Concrete Frames

* Keh-Chyuan Tsai[1)], An-Chien Wu[2)], Kuan-Yu Pan[3)], Hsun-Horng Yang[4)]

[1), 3), 4)] *Dept. of Civil Engineering, Nat'l Taiwan University, Taipei 10617, Taiwan*
[2)] *National Center for Research on Earthquake Engineering, Taipei 10617, Taiwan*

[1)] kctsai@ntu.edu.tw, [2)] acwu@ncree.narl.org.tw
[3)] r01521219@ntu.edu.tw, [4)] r01521219@ntu.edu.tw

ABSTRACT

This paper introduces a method of retrofitting reinforced concrete (RC) frames with buckling-restrained braces (BRBs) and a novel implementation of BRBs in new RC frame construction. In the retrofitted buildings, instead of the traditional post-installed anchors, load is transferred between the BRB and RC frame through compression bearing between an installed steel frame connected to the BRB, and high-strength mortar blocks constructed at the four corners of the RC frame. This avoids complex on-site anchor installation, and does not limit the allowable brace force by the anchor strength. Cyclic increasing displacements were imposed on two RC frame specimens retrofitted with different BRB strength capacities. Test results indicate that the proposed method efficiently transferred loads between the BRBs and RC frames, increasing the frame lateral strength while achieving good ductility and energy-dissipating capacity. When the bearing block was reinforced with wire mesh, the maximum frame lateral strength and stiffness were more than 2.2 and 3.5 times the RC frame without the BRB respectively.

Regarding BRB application to new RC frames, seismic design and analysis methods for using a proposed steel cast-in anchor bracket (CAB) to transfer normal and shear forces between the BRB and RC members are investigated. A full-scale two-story RC frame with BRBs (BRB-RCF) was tested using hybrid and cyclic loading test procedures. The BRBs were arranged in a zigzag configuration and designed to resist 70% of the story shear. Test results confirm that the BRBs enhanced the RC frame stiffness, strength, and ductility. The hysteresis energy dissipation ratios in the four

---

[1)] Professor
[2)] Assistant Research Fellow
[3)] Research Assistant

hybrid tests range from 60% to 94% in the two stories, indicating that BRBs can effectively dissipate seismic input energy. No failure of the proposed steel CABs and RC discontinuity regions (D-regions) was observed.

1. INTRODUCTION

Many studies have shown that BRBs effectively provide high stiffness, strength, and seismic resilience (Lin *et al.* 2012; Mahrenholtz *et al.* 2015; Pan *et al.* 2016; Tsai *et al.* 2008; Tsai and Hsiao 2008; Tsai *et al.* 2014), leading to their wide adoption in new construction and retrofitting of steel buildings. BRBs are less common in RC structures, because of the difficulties of transferring large forces between the BRB and RC members. There are various benefits to using BRBs in RC moment frames, including the reduction in RC member sizes and increased lateral stiffness and energy dissipation, which reduces the building weight and allows for greater architectural flexibility, while reducing the drift of the structure during a severe earthquake. The bracing methods adopted in practice for RC structures fall into two main categories, namely the direct and indirect systems. In the direct system, the brace is directly connected to the RC frame through anchor brackets (Mahrenholtz *et al.* 2015). Brace load capacity is therefore limited by the anchorage since the brace force is concentrated at the anchor brackets. In the indirect system, a braced steel frame is installed inside the RC frame with closely-spaced post-installed anchors used to connect the steel and RC frames (Ishimura *et al.* 2012). As a result, load transfer between the brace and RC frame is achieved indirectly through the steel frame. The distribution of brace force over the length of the steel frame members increases the anchorage capacity and enables the use of larger braces compared to the direct system. However, grouting of the continuous interface between the steel and RC frames is technically challenging and is a potential location of failure. Furthermore, post-installed anchors are commonly designed with a high degree of redundancy because of the lack of precise and verified design models. This results in high cost and construction times because of substantial on-site drilling and anchor installation. In addition, the uncertain interaction between the RC and steel frames is also undesirable and leads to difficulty in structural design and analysis.

This research utilizes high-strength mortar bearing blocks constructed at the four corners of the RC frame to transfer load between the steel and RC frames (Pan *et al.* 2016). The use of bearing blocks was first proposed as a retrofit solution by Paret (2007) to avoid the redundancy of post-installed anchors and to simplify the interaction between the RC and steel frames. The system also does not limit the brace load capacity by the anchorage capacity. Without prior experimental evidence of this approach, cyclic testing of two full-scale RC frames retrofitted with identical steel frames but with different BRB load capacities were conducted in this study.

For the implementation of BRBs in new RC frames, an I-shaped steel anchor brackets cast into RC members to connect the BRB and RC frame are proposed (Wu *et al.* 2016). When the BRB is in tension, the tensile forces are transferred to the RC member through the steel CAB, thus avoiding dependence on the tensile pullout strength of the anchors. In order to develop a steel CAB system design and construction procedure and investigate the proposed system performance under severe

earthquakes, hybrid tests using four earthquake ground motions followed by cyclic loading tests were conducted on a full-scale two-story BRB-RCF specimen.

2. EXPERIMENTAL PROGRAM

Weld end-slot BRBs (WES-BRBs) as shown in Fig. 1 were adopted in this study. Gussets in the specimens were designed using the uniform force method (Thornton 1991) to distribute BRB axial actions to the gusset-to-steel frame member interfaces. Details of the design checks for the BRBs and connections, including the BRB steel casing flexural buckling, joint region tension yielding, joint region compression buckling, gusset tension yielding or compression buckling, and gusset interface strength were performed according to Chuang *et al.* (2015).

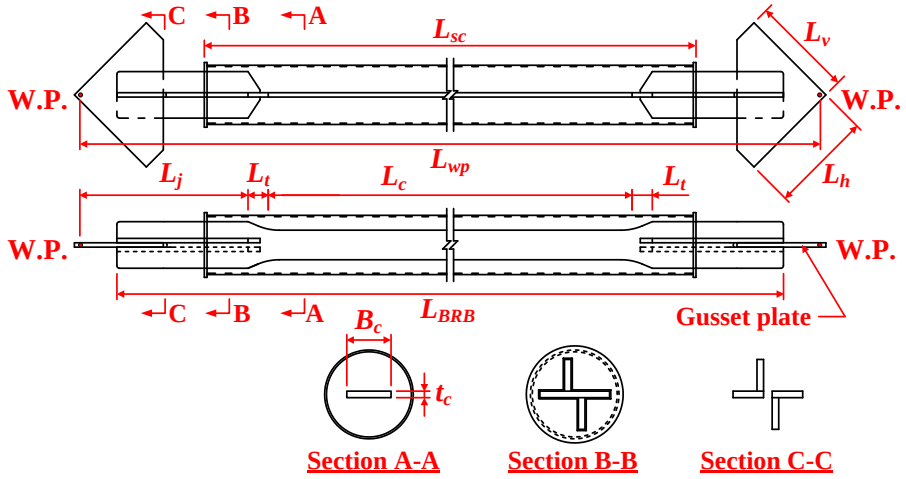

Fig. 1 Profiles of the WES-BRB and connections

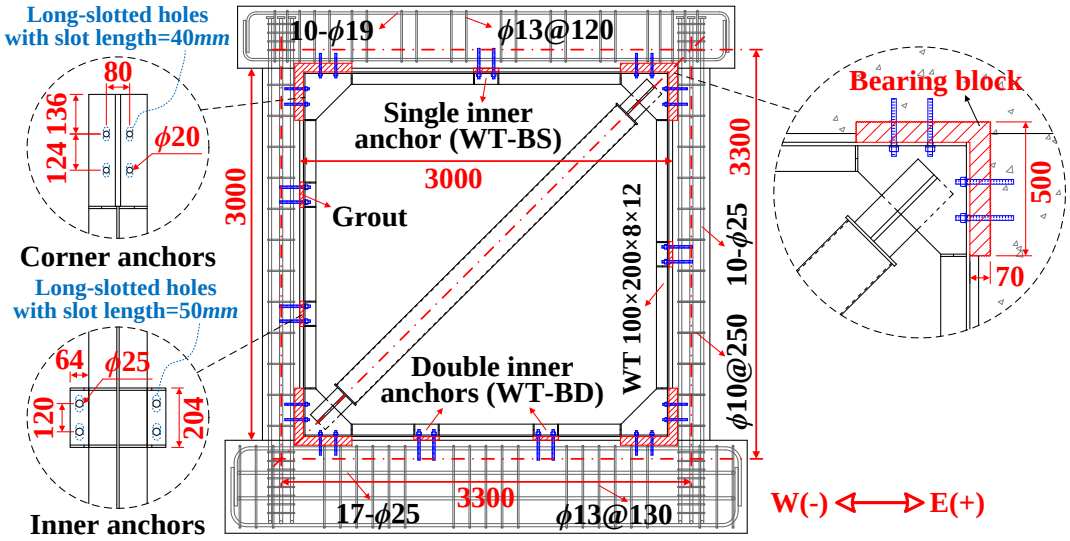

Fig. 2 Dimensions and reinforcement layout of the retrofitted frame

2.1 Design for Existing RC Frame with BRBs

2.1.1 Design concept and retrofitting objective

Performance-base design can be adopted to optimize the target responses of the retrofitted structure based on the limitation of allowable inter-story drift and base shear increase. In this study, an example of maximizing the lateral strength, stiffness and ductility of a single-bay RC frame using the proposed buckling-restrained braced frame (BRBF) and bearing block load transfer mechanism (Pan *et al.* 2016), while preventing failure in the RC members and beam-column joints, is illustrated. The BRBF comprises the steel frame and BRB, while the bearing blocks are constructed at the four corners of the RC frame (Fig. 2) to transfer loads between the RC frame and BRBF. When the RC frame displaces laterally during an earthquake, the new BRBF is loaded through the bearing blocks at the corners. For the brace in compression, the bearing blocks adjacent to the brace ends transfer forces directly from the RC frame to the BRBF with insignificant demands in the steel frame members. For the brace in tension, the bearing blocks opposite to the brace ends transfer loads from the RC frame to the steel frame, which then transfers the forces in compression to the brace ends. The steel frame members are therefore designed as compression members to resist the force demands when the maximum brace tensile strength develops.

2.1.2 Design of the retrofitted RC frame specimen

Two identical RC frames were retrofitted with identical steel frames but with different BRB capacities (specimens WT-BS and WT-BD) to investigate the load transfer mechanism and seismic performance of the proposed method. The RC frame specimens represent the first story RC beam-to-two columns frame subassembly in the typical Taiwanese old school buildings. Both the story height and bay width of the RC frame specimens were 3300mm as shown in Fig. 2. The reinforcements of the RC members were considered non-ductile in modern seismic standards. The nominal yield strengths of the longitudinal and transverse reinforcing bars were 420MPa and 280MPa respectively. The design concrete compressive strengths were 21MPa for the RC columns and top beam, and 42MPa for the foundation. The BRB steel cores were fabricated from ASTM A572 GR50 steel plate (345MPa nominal yield stress). The BRB core cross-sections of specimens WT-BS and WT-BD were 16×108mm and 16×85mm respectively. The restrainers in specimens WT-BS and WT-BD were fabricated from 216.3×4mm and 190.7×4mm circular pipes respectively. The gusset thickness was 18mm using A572 GR50 steel. Four 100×200×8×12mm WT shape members (A572 GR50 steel) were adopted for each steel frame. The webs at both ends of the WT members were removed to provide space for the gussets. This allowed the WT member flange to be continuous at the interface between the WT member web and gusset. In order to increase the WT member compression buckling capacity, inner anchors (Fig. 2) were installed to reduce the WT member unbraced length. Buckling in both the frame out-of-plane and in-plane directions was considered. The letters “S” and “D” of the specimen identifications, WT-BS and WT-BD, represent the WT member constrained by single and double inner anchor groups respectively. In order to prevent BRB end instability in the out-of-plane direction, both ends of the WT members were restrained by the corner anchor groups.

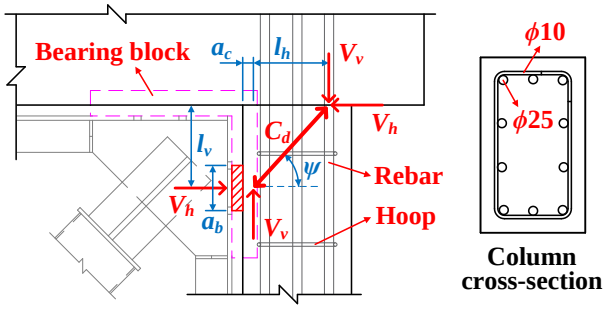

Fig. 3 Softened strut-and-tie model for the RC column top D-region

Loading of the BRBF occurs through the bearing blocks installed at the four corners of the RC frame. The bearing block was constructed using the non-shrink mortar with a design compressive strength of 56MPa. The BRBF was placed into the RC frame after removing the concrete covers at the four frame corners. Consequently, the typical clearance between the RC members and BRBF was about 30mm. The formwork was then constructed for grouting the mortar at the four corners and around the inner anchors. It is expected that the load transfer between the RC frame and BRBF will be no longer effective when the bearing block is severely cracked or crushed. In order to investigate a possible method to mitigate the possible damage, the bearing blocks in specimen WT-BD were reinforced with 40×40mm wire mesh (2.5mm in diameter). The simplified procedure using the soften strut-and-tie (SST) model proposed by Hwang and Lee (2002) was adopted to evaluate the shear capacities of the RC member D-regions (Fig. 3) to resist the additional local shear demand induced by the BRBF through the bearing blocks.

2.1.3 Test setup and loading protocol

The top beam of the RC frame was sandwiched by two steel cross beams with tensioned rods (Fig. 4(a)). The lateral forces from the servo-hydraulic actuators were transferred to the RC frame through the steel cross beams. In order to simplify the test setup, no vertical load was applied to simulate the gravity load effect. Consequently, the flexural and shear resisting capacities of the RC columns were reduced. The RC column responses were expected as the lower bound performance of a real RC structure. A separate linear displacement transducer at the east side of the specimen was used to measure the RC frame lateral deformation for the displacement control of actuators. The steel frame lateral deformations were measured by two displacement transducers installed at both sides of the steel frame. The BRB axial deformations were measured from the relative displacement between the steel core end and the steel casing by two displacement transducers (four in total) mounted at each end of the BRB. In order to compute the BRB forces, eight strain gauges (16 in total) were attached at the BRB end elastic sections. Each segment of the east vertical and bottom horizontal WT member sections were instrumented with four and two strain gauges on its flanges and web respectively to measure the WT member axial forces. The specimens were subjected to a sequence of displacement-controlled cycles (Fig. 4(b)) comprising three cycles each to drift ratios starting from 0.125% and increasing to 5.0%, as prescribed in ACI 374.1-05 (2005).

(a)

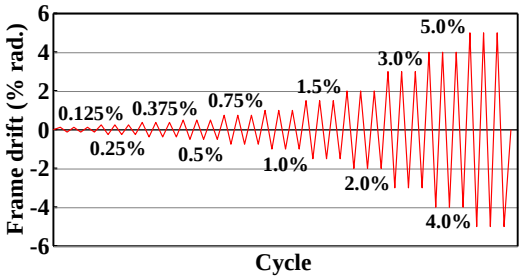

(b)

Fig. 4 (a) Test arrangement and (b) loading history

2.2 Design for New RC Frame with BRBs

2.2.1 Seismic design principles of the BRB-RCF

The proposed RC frame is required to undergo large deformation without significant loss of strength and stiffness and was therefore designed as a special moment frame in accordance with ACI 318-14 (2014). This includes the strong column-weak beam capacity design to ensure that controlled yielding occurs at the beams adjacent to the gusset plates and column faces and at the column bases. Depending on the BRB's material grade, the inclination angle, and the length ratio of the core yield region to the distance from work point to work point, the BRB may start to yield at an inter-story drift ratio (IDR) of less than 0.3% (Tsai *et al.* 2014). In this study, the BRBs were designed to yield at a target displacement, while the RC members were designed to remain elastic until the BRBs reached their yield strength. After this point, yielding at the beam ends commences and eventually leads to the development of full plastic hinges at the beam ends and column bases. The beam-column joints and proposed steel CABs were designed to remain elastic when the BRBs reach their maximum load demands. Tension and shear failures of the RC members and shear failure of the RC member D-regions in the beam-column joints and steel CAB regions were suppressed through capacity design.

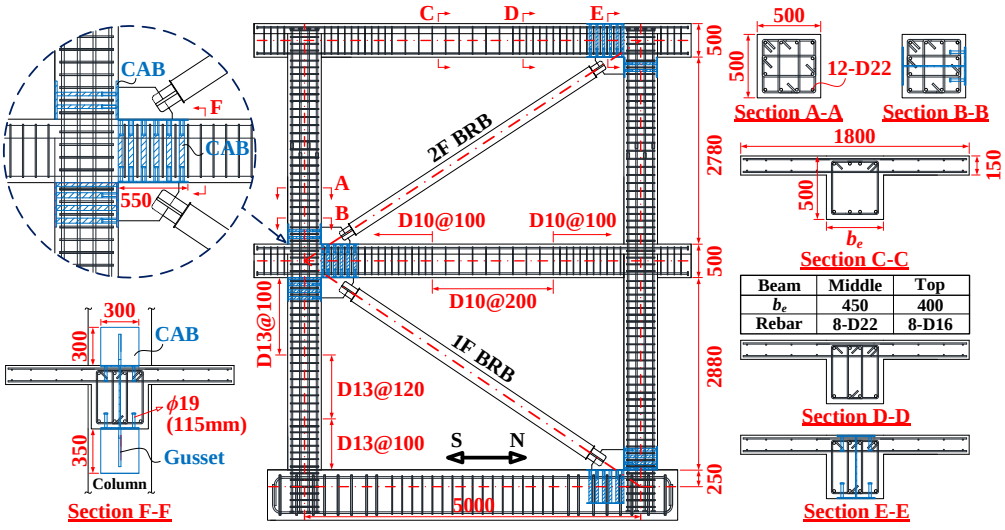

Fig. 5 Elevation of the BRB-RCF specimen

2.2.2 Design of the two-story BRB-RCF specimen

The test specimen (Fig. 5) was designed to reflect typical RC frame construction with a bay width of 5000mm and a total height of 7410mm, which comprised the first and second story heights of 3380mm and 3280mm, respectively, and a foundation beam 750mm in depth (Wu *et al.* 2016). The BRB steel cores were fabricated using ASTM A36 steel, which has a nominal yield stress of 250MPa. The BRB core cross-sectional areas were 3240mm^2 and 2120mm^2 for the first and second stories, respectively, designed based on the target axial yield strength and effective stiffness ratios of 3:2 and the available actuator capacities. The BRB restrainers for the first and second stories were, respectively, fabricated from 216.3×4.5mm and 190.7×4.5mm circular pipes filled with 56-MPa non-shrink mortar. The BRBs were arranged in a zigzag configuration, with the ends of the two BRBs at adjacent stories connected in the same beam-column connection, to reduce the axial load demands in the RC beams.

The RC frame member sizes were chosen to ensure the BRB resists approximately 70% of the story shear at BRB first yield. The beams were then designed to yield when the BRB axial load reached 0.9Py, with a strength reduction factor of 0.9 applied. The other frame elements, including the beam shear reinforcements, beam-column joints, and column longitudinal reinforcements, were then detailed as a special moment frame in accordance with ACI 318-14, and therefore undergo a strong column-weak beam failure mechanism. Each RC beam was built integrally with a 150-mm-thick and 1800-mm-wide floor slab to create a T-section to simulate floor slab effects. In order to prevent shear failure in the RC members, the transverse reinforcements in the beams and columns were designed and detailed to meet ACI 318-14 ductile design requirements for the special moment frame. The design concrete compressive strength was 35MPa for the RC frame, while the longitudinal and transverse reinforcing steel had a nominal yield stress of 420MPa. The steel CABs and BRB gussets were fabricated with A572 GR50 steel.

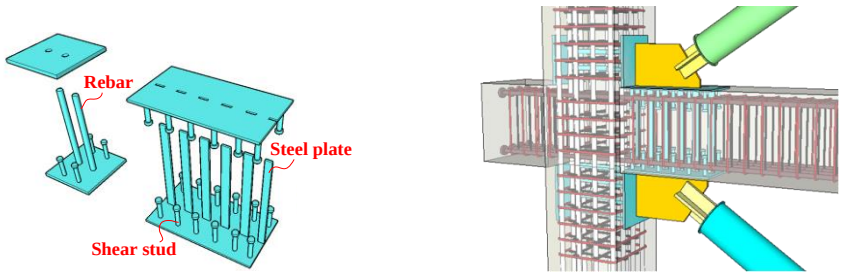

Fig. 6 Schematics of the steel CAB

2.2.3 Design of steel CABs

The schematics of the proposed steel CAB and a 3D view of the assembled connection are shown in Fig. 6. Two CABs are adopted for each gusset, one installed through the column and the other through the beam, with the gusset plate welded onto the two perpendicular CABs. Each I-shaped steel CAB comprises two flange plates that are installed on either side of the associated RC member and connected to each other through tension ties as a web, and shear studs welded onto the inside of the flange plates. The flange plates provide a steel interface for the BRB gusset connection. The connections between the steel CAB and RC member were designed to resist the

combined shear and normal loads induced by the BRB and frame action effects. The shear forces were designed to be transferred to the RC members through shear studs. The normal forces were designed to be transferred into the RC member D-regions through compression bearing on the concrete. The tension ties were designed to prevent the steel from tension yielding and rupture. The welds between the tension ties and flange plates were also designed to resist the tension force from the BRB.

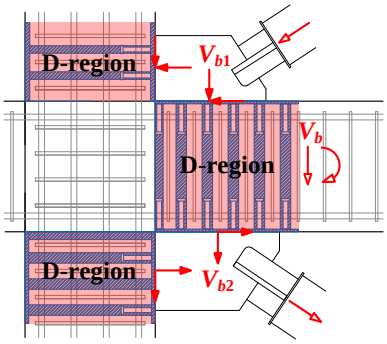

(a)

(b)

Fig. 7 (a) Illustration of the D-regions in RC members and (b) test setup

2.2.4 Design of D-regions in RC members

As shown in Fig. 7(a), the loads from the gusset plates are transmitted to the RC columns and beams at locations of approximately half the gusset height and length, respectively. They act as large concentrated loads at the beam and column ends, and are thus categorized as D-regions. The force demand for the D-region in the beam end, for example, is the combined loads from the BRB and frame action effects and also the beam shear force. The shear demand in the beam is evaluated from the beam's plastic hinges formed at the gusset edge and column face. Because of the zigzag configuration of the coupled gusset shown in Fig. 5, the shear forces in the D-region are larger as both BRBs act in the same direction. For the D-regions in the RC columns, the column shear forces involved in the combined force demands were computed at the frame ultimate state when the plastic hinges form at the beam ends and column bases. The D-region design capacity was evaluated using the simplified method of the SST model (Hwang and Lee 2002).

2.2.5 Test setup and procedures

The BRB-RCF specimen was oriented in the north-south direction with the actuators in the south (Fig. 7(b)). In order to simulate the gravity load effects, a loading system using post-tensioned rods was employed by applying around 2550kN to each column. Two steel transfer beams attached to each outer end of the T-shaped RC floor beam were connected to each other by applying 589kN post-tension for each floor. The lateral forces from three electro-servo hydraulic actuators at each floor were transferred to the specimen through contact bearing of the transfer beam. Each of the two steel transfer beams in the north end of the specimen was anchored to the RC beam using pre-installed bolts. In this manner, gaps would never develop between the north transfer beam and the RC beam end during the tests. Subsequently, a separate high-

precision digital displacement encoder was installed outside the north steel transfer beam at each floor for displacement control of the actuators.

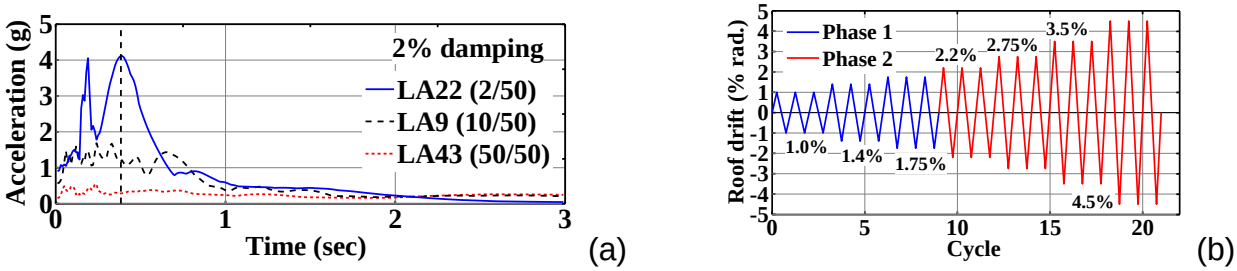

Fig. 8 (a) 2% damped elastic response spectra and (b) cyclic loading protocol

In order to investigate the seismic responses of the BRB-RCF specimen, a total of 60 ground motions with hazard levels of SLE, DBE and MCE, as adopted in the SAC research project (Gupta and Krawinkler 1999), were considered when conducting nonlinear response history analyses using PISA3D program (Lin *et al.* 2009). A fundamental period of approximately 0.384s resulted from assigning a mass of 0.225kN-s^2/mm for each floor. Rayleigh damping considering first- and second-mode damping ratios of 2% was specified in the analytical model. Analysis results showed that the LA43 (SLE), LA09 (DBE), and LA22 (MCE) earthquakes' force and displacement demands on the BRB-RCF specimen would be within the capacity of the NCREE laboratory facilities. Fig. 8(a) shows the 2% damped elastic response spectra of the three earthquake hazards. Four hybrid tests were conducted using the ground motions at the SLE, DBE, and MCE levels in sequence. The earthquake of MCE level was imposed on the BRB-RCF twice to simulate a strong aftershock event. After the hybrid tests, the specimen was subjected to a sequence of cycles (Fig. 8(b)) comprising three cycles each with drift ratios starting from 1.0% and increasing to 4.5%, as prescribed in ACI 374.1-05. In Phase 1 of the cyclic loading test, displacement-controlled loadings were applied to the roof floor and the actuators at the second floor were force controlled according to the proportion of an inverted-triangular force distribution along the height of the specimen. After the loadings of the 1.75% roof drift ratio, the displacement control mode in Phase 2 of the cyclic loading test was applied on both floors to make the IDRs in both stories identical.

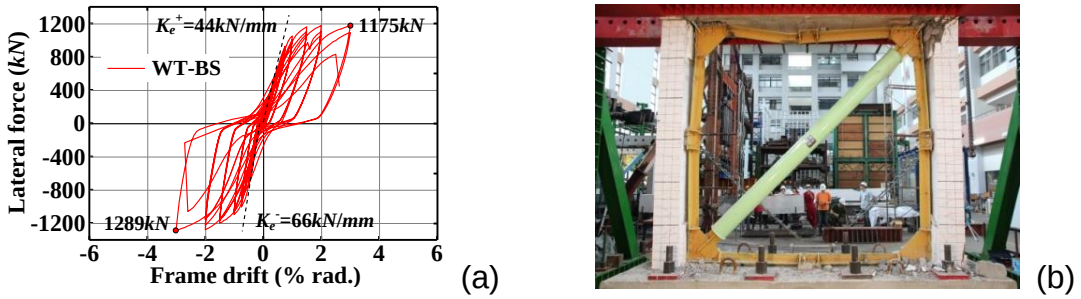

Fig. 9 Specimen WT-BS (a) experimental force-deformation response and (b) damage conditions at the end of test

3. EXPERIMENTAL RESPONSES

3.1 RC Frames Retrofitted with BRBs

Specimen WT-BS At the first loading cycle to 3.0% radian drift, the maximum lateral strengths of specimen WT-BS were 1175kN (BRB in tension) and 1289kN (BRB in compression) as shown in Fig. 9(a). Because of gaps developing between the RC frame and BRBF corners as well as the WT member axial deformation, the specimen lateral elastic stiffness K_e^-=66kN/mm (BRB in compression) is about 1.5 times that of K_e^+=44kN/mm (BRB in tension). It also resulted in pinching of the force-deformation response. Shear failure occurred at the east RC column top (Fig. 9(b)) at -2.7% radian drift during the second 3.0% radian drift cycle. During the third cycle to 3.0% radian drift, the top horizontal WT member buckled in the vertical direction at +2.7% radian drift because of the inner anchor failure. The crack in the severe shear failure of the column top was extended to the top beam in the following cycles.

Specimen WT-BD The bearing blocks were reinforced by the wire mesh, and thus improved the frame ductility and serviceability by reducing cracking or crushing. The improved load transfer between the RC frame and BRBF is shown by their similar drifts even under large lateral deformations. However, minor gaps did develop between the RC frame and BRBF corners, which resulted in the slight difference in lateral elastic stiffness between the BRB in compression (K_e^-=42kN/mm) and tension (K_e^+=35kN/mm). Figure 10(a) shows the stable hysteresis responses of specimen WT-BD without the pinching behavior seen in specimen WT-BS. The maximum lateral strengths were 891kN (BRB in tension) and 1018kN (BRB in compression) at the first 3.0% radian frame drift cycle. Plastic hinges formed at both ends of the RC column (adjacent to the bearing block edges), and at both ends of the vertical WT members (adjacent to the gusset edges). During the second cycle to 5.0% radian drift, the BRB steel core fracture resulted in the sudden drop in the frame lateral resistance. The failure mode of the RC columns is categorized as the flexural-shear failure (Fig. 10(b)).

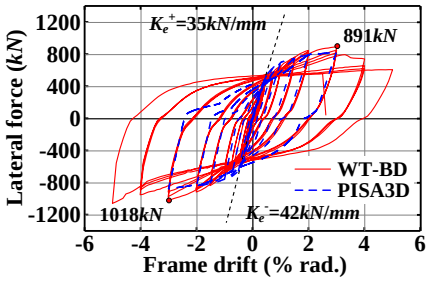

(a)

(b)

Fig. 10 Specimen WT-BD (a) experimental force-deformation response and (b) damage conditions at the end of test

Figure 11(a) compares the force-deformation response envelopes of the three specimens with the bare RC frame specimen PF (Mahrenholtz *et al.* 2015). The similar force-deformation responses of specimens WT and PF indicate that the WT steel frame provided insignificant contribution to the lateral resistance. The lateral resistance of the retrofitted specimens WT-BS and WT-BD increased by more than 2.8 and 2.2 times that of specimen WT respectively. Figure 11(b) compares the specimen degradation

evaluated based on the peak-to-peak stiffness at the third cycle of each drift level. The lateral stiffness of specimens WT-BS and WT-BD was approximately 4.5 and 3.5 times that of specimen WT respectively. The rate of stiffness degradation for specimens WT-BS and WT-BD was almost equal until the 3.0% radian drift cycles. The WES-BRBs in specimens WT-BS and WT-BD exhibited satisfactory performance with stable and repeatable hysteresis behavior. Both BRBs in specimens WT-BS and WT-BD resisted about 56% of the base shear when the BRBs developed their full compressive strengths. The WT frame effectively transferred the loads from the RC frame to the BRBF in compression. The anchors effectively prevented buckling by reducing the unbraced lengths of the WT members in both buckling directions. Figures 12(a) and 12(b) present the axial force responses of the east vertical and bottom horizontal WT members measured by the installed strain gauges for specimen WT-BS. In specimen WT-BD, similar force responses were found in the east vertical and bottom horizontal WT members (Figs. 13(a) and 13(b)). Test results confirm that the expected load transfer mechanism has been achieved in the specimens. For practical applications, it is recommended that the anchor holes in the flanges of WT members be designed and fabricated as long-slotted holes in order to prevent the failure of the proposed anchoring system and the force transfer mechanism.

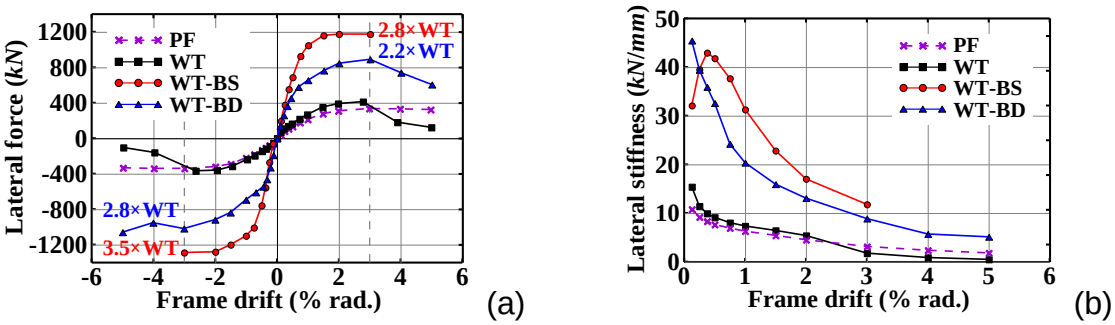

Fig. 11 (a) Lateral force-drift response envelopes and (b) lateral stiffness degradation with respect to drift

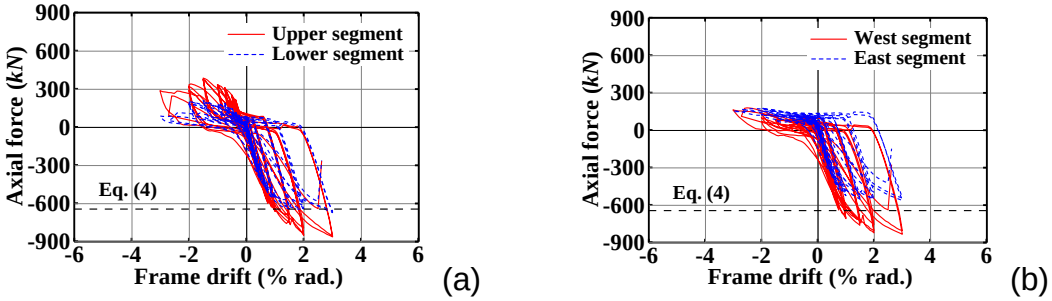

Fig. 12 Axial force responses of (a) east vertical and (b) bottom horizontal WT members for specimen WT-BS

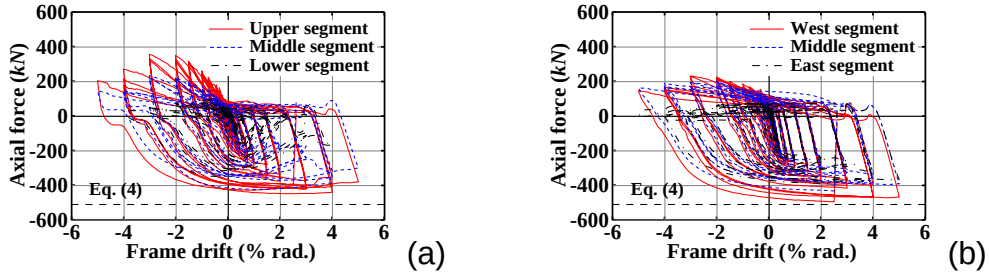

Fig. 13 Axial force responses of (a) east vertical and (b) bottom horizontal WT members for specimen WT-BD

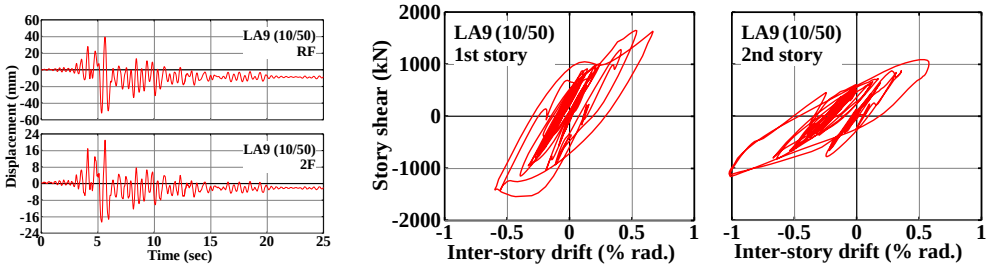

Fig. 14 Floor displacement histories and the story shear versus story drift relationships in the DBE test

3.2 Two-story BRB-RCF specimen

The peak base shear and IDR in the first story were, respectively, 1000kN and 0.22%, while the peak story shear and IDR in the second story were, respectively, 580kN and 0.2% during the SLE test. The linear story shear versus story drift relationships in both stories indicate that the BRB-RCF remains elastic. During the DBE test, the BRB-RCF went into inelastic range and exhibited good seismic performance with stable hysteresis behavior as shown in Fig. 14. The maximum base shear reached 1600kN and the peak IDR in the second story was twice as large as that in the first story. The difference in IDR between the two stories gradually became obvious and the second story drift responses were unsymmetrical for the two directions. In the MCE-1 test (Fig. 15), the peak base shear was 1750kN and the second story peak IDR was still twice as large as that in the first story. The negative drift responses were significantly larger than the positive ones in both stories.

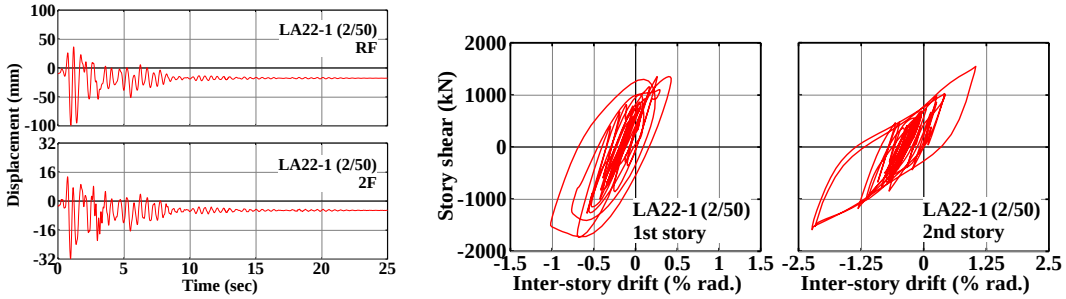

Fig. 15 Floor displacement histories and the story shear versus story drift relationships in the MCE-1 test

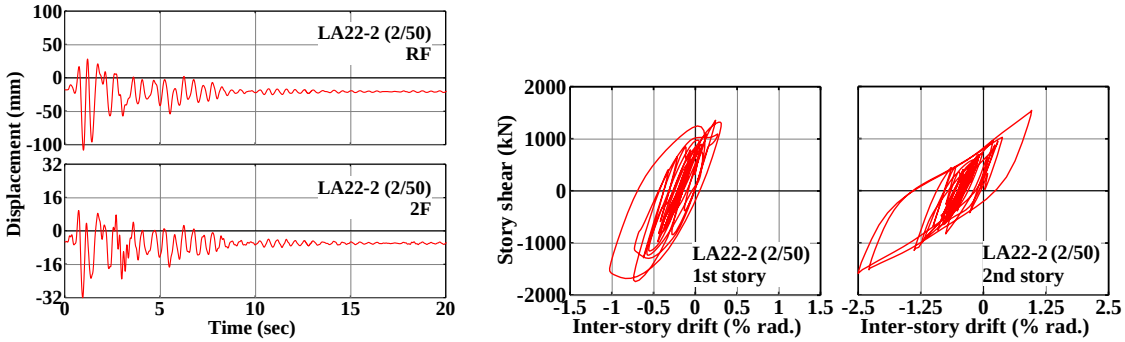

Fig. 16 Floor displacement histories and the story shear versus story drift relationships in the MCE-2 test

As shown in Fig. 16, the overall frame responses in the MCE-2 test were similar to those in the previous one. Comparing Figs. 15 and 16, the cyclic story shear versus IDR performances of the specimen are found remarkably similar in the MCE-1 and MCE-2 tests. This suggests the robustness of the proposed BRB-RCF when subjected to severe earthquake shocks. Figure 17 shows the experimental story shear versus IDR relationships in the Phase 1 and Phase 2 cyclic loading tests. The reinforcing bars at both ends of the top and middle beams (outside the CAB regions) yielded during the MCE-1 test. During the 1.4% roof drift level in the Phase 1 cyclic loading test, all the reinforcing bars at both column bases yielded. At the end of the test, no reinforcing bars at the tops and middles of the columns yielded. It is confirmed that locations and time instances of plastic hinge formation in the BRB-RCF were in accordance with the design expectations. During the second and third loading cycles of 3.5% IDR, the longitudinal reinforcing bars fractured at the bottom of the top beam ends, leading to the decrease in the second story shear.

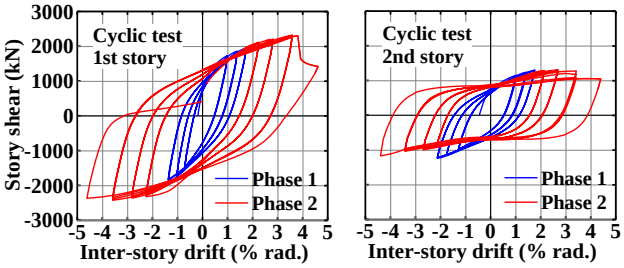

Fig. 17 Story shear versus inter-story drift relationships in the Phase 1 and Phase 2 cyclic loading tests

Figure 18 shows the energy dissipated by the BRBs and by the entire structural system in each story during various tests. During the three hybrid tests, the energy dissipation ratios for the second story BRB were more than 90%, while the ratios ranged from 60% to 73% for the first story BRB. The energy dissipation ratios during the cyclic loading test were calculated until the end of the 2.75% IDR loading cycles, owing to the failure of the BRB strain gauges. Both BRBs absorbed around 70% of the dissipated energy in the entire structural system during the cyclic loading test. Test results suggest that the

BRBs could effectively dissipate seismic input energy at various seismic hazard levels, while the moment-resisting frame would need to dissipate a significant amount of energy only during strong earthquakes. Figure 19 shows the first- and second-story lateral stiffness degradations evaluated based on the peak displacement at each hybrid test and the peak-to-peak stiffness at the third cycle of each drift level (except the 4.5% IDR loading cycle) during the cyclic loading tests. In the figure, the lateral secant stiffness of the RC frame is calculated by subtracting the BRB lateral secant stiffness from that of the BRB-RCF. All the lateral secant stiffnesses are normalized by the corresponding elastic story stiffnesses, K_{E1}=145 kN/mm and K_{E2}=90kN/mm computed from the SLE test. Figure 20(a) shows the yield locations and time instances of the longitudinal reinforcing bars in the RC members. Except for the failed strain gauges on the reinforcing bars at the south end of the middle beam, the reinforcing bars at both ends of the top and middle beams (outside the CAB regions) yielded during the MCE-1 test. During the 1.4% roof drift level in the Phase 1 cyclic loading test, all the reinforcing bars at both column bases yielded. Damage conditions of the columns at +3.5% IDR are shown in Figs. 20(b) and 20(c), which indicate that concrete spalling occurred at beam ends and column bases as expected. At the end of the test, no reinforcing bars at the top and middle of the columns yielded. The locations and instances of plastic hinge formation in the BRB-RCF were in accordance with the design expectations.

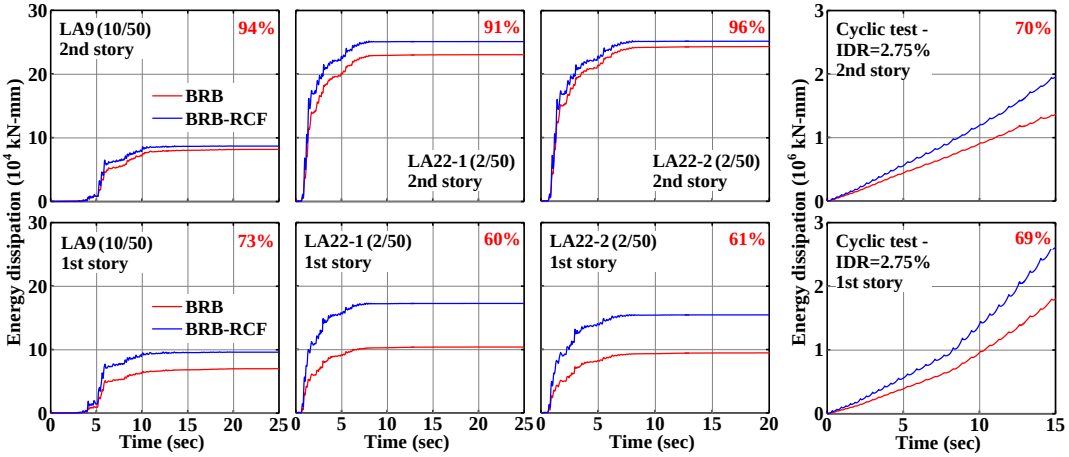

Fig. 18 Dissipated energy in BRBs and entire structural system during various tests

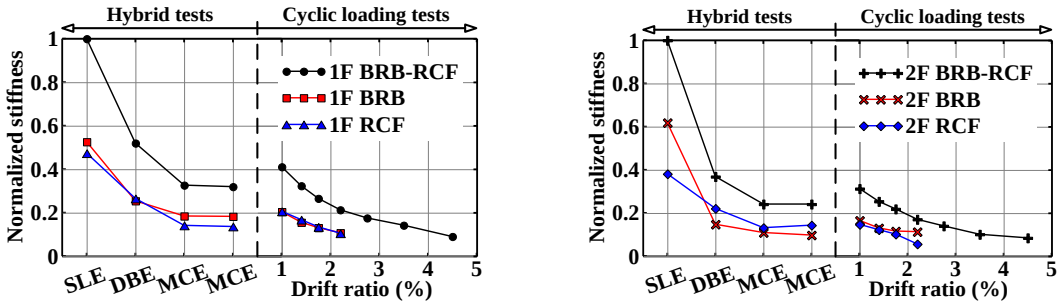

Fig. 19 Normalized lateral stiffnesses for the first and second stories

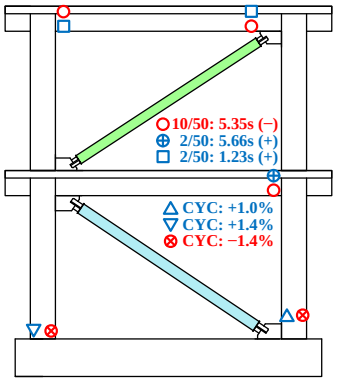

(a)

(b)

(c)

Fig. 20 (a) Rebar yield locations and time instances, (b) south and (c) north RC member damage conditions at IDR = +3.5%

4. CONCLUSIONS

Based on the cyclic loading tests of the retrofitted RC frames with BRBs, the following conclusions can be drawn:

(1) The proposed retrofitting system transfers load between the RC frame and BRBF through compression bearing at high-strength mortar blocks constructed at the four corners of the RC frame.
(2) Experimental results showed the viability of the proposed system. The behavior corresponded well to the design expectation, where seismic energy was dissipated primarily through BRB yielding and plastic hinges formed at both ends of the RC columns and steel frame members.
(3) The WES-BRBs in specimens WT-BS and WT-BD exhibited satisfactory performance with stable and repeatable hysteresis behavior without end connection instability. The maximum lateral resistance contributed by the BRBs accounts for 56% of the total lateral resistance.
(4) Cracking in bearing blocks can be mitigated by wire mesh reinforcing, which improves load transfer and hence overall ductility and serviceability of the retrofitted frame. This was shown in specimen WT-BD which exhibited satisfactory and stable hysteresis behavior without significant pinching behavior.
(5) The proposed retrofitting system can be designed to prevent unexpected failure occurred in the RC beams, columns and beam-column joints. The simplified approach of SST model effectively and conservatively evaluated the shear capacities in the RC member D-regions to resist the additional local shear demand induced by the BRBF through the bearing blocks.

From the full-scale two-story BRB-RCF hybrid and cyclic loading tests, the following conclusions can be drawn:

(1) The proposed steel CABs allow the installation of reinforcements for RC members without interference. The procedure for construction of a BRB-RCF specimen demonstrated in this study shows the feasibility of the proposed system for practical applications.
(2) Test results confirm that a properly designed and constructed BRB-RCF can satisfy the design objectives for seismic performance and maintain satisfactory seismic behavior, even after a two severe earthquakes.
(3) The design methodologies for the BRB-RCF proposed in this study ensure that the BRBs yield first. The locations and time instances of the ensuing plastic hinge formation in the BRB-RCF beams and column bases are in accordance with the design expectations.
(4) The proposed steel CABs performed very well without failure and the tension ties of the

CABs were subjected to tension without yielding throughout the entire series of tests as expected. This suggests that the seismic performance of the BRB and RC frame can be assured by using the proposed design method for the CABs.

(5) During the hybrid tests, the BRBs resisted 52% to 71% of the story shears, showing that the BRBs could effectively provide the frame lateral resistance and stiffness.

(6) The two WES-BRBs dissipated 60% to 96% of the total input energy in various tests, demonstrating that the BRB could effectively absorb most of the input earthquake energy in an RC frame.

REFERENCES

American Concrete Institute (ACI). (2005), "Acceptance Criteria for Moment Frames Based on Structural Testing and Commentary (ACI 374.1-05)," *ACI*, Farmington Hills, Michigan.

American Concrete Institute (ACI). (2014), "Building Code Requirements for Structural Concrete and Commentary (ACI 318-14)," *ACI*, Farmington Hills, Michigan.

Chuang, M.C., Tsai, K.C., Lin, P.C. and Wu, A.C. (2015), "Critical limit states in seismic buckling-restrained brace and connection designs," *Earthquake Engineering and Structural Dynamics*, **44**(10), 1559-1579.

Gupta, A. and Krawinkler, H. (1999), "Seismic Demands for Performance Evaluation of Steel Moment Resisting Frame Structures (SAC Task 5.4.3)," *John A. Blume Earthquake Engineering Center: Report No. 132*, Department of Civil and Environmental Engineering, Stanford University, Stanford, California.

Hwang, S.J. and Lee, H.J. (2002), "Strength prediction for discontinuity regions by softened strut-and-tie model," *Journal of Structural Engineering*, **128**(12), 1519-1526.

Ishimura, M., Sadasue, K., Miyauchi, Y., Yokoyama, T., Fujii, T. and Minami, K. (2012), "Seismic performance evaluation for retrofitting steel brace of existing RC building with low-strength concrete," *The Fifteenth World Conference on Earthquake Engineering*, Lisbon, Portugal.

Lin, B.Z., Chuang, M.C. and Tsai, K.C. (2009), "Object-oriented development and application of a nonlinear structural analysis framework," *Advances in Engineering Software*, **40**(1), 66-82.

Lin, P.C., Tsai, K.C., Wang, K.J., Yu, Y.J., Wei, C.Y., Wu, A.C., Tsai, C.Y., Lin, C.H., Chen, J.C., Schellenberg, A.H., Mahin, S.A. and Roeder, C.W. (2012), "Seismic design and hybrid tests of a full-scale three-story buckling-restrained braced frame using welded end connections and thin profile," *Earthquake Engineering and Structural Dynamics*, **41**(5), 1001-1020.

Mahrenholtz, C., Lin, P.C., Wu, A.C., Tsai, K.C., Hwang, S.J., Lin, R.Y. and Bhayusukma, M.Y. (2015), "Retrofit of reinforced concrete frames with buckling-restrained braces," *Earthquake Engineering and Structural Dynamics*, **44**(1), 59-78.

Pan, K.Y., Wu, A.C., Tsai, K.C., Li, C.H. and Khoo, H.H. (2016), "Seismic retrofit of reinforced concrete frames using buckling-restrained braces with bearing block load transfer mechanism," *Earthquake Engineering and Structural Dynamics*, **45**(14), 2303-2326.

Paret, T.F. (2007), "Brace for the Big One," *Modern Steel Construction*, August, American Institute of Steel Construction, Chicago, Illinois.

Thornton, W.A. (1991), "On the analysis and design of bracing connections," *National Steel Construction Conference*, American Institute of Steel Construction, Chicago, Illinois.

Tsai, K.C., Hsiao, P.C., Wang, K.J., Weng, Y.T., Lin, M.L., Lin, K.C., Chen, C.H., Lai, J.W. and Lin, S.L. (2008), "Pseudo-dynamic tests of a full-scale CFT/BRB frame—Part I: Specimen design, experiment and analysis," *Earthquake Engineering and Structural Dynamics*, **37**(7), 1081-1098.

Tsai, K.C. and Hsiao, P.C. (2008), "Pseudo-dynamic tests of a full-scale CFT/BRB frame—Part II: Seismic performance of buckling-restrained braces and connections," *Earthquake Engineering and Structural Dynamics*, **37**(7), 1099-1115.

Tsai, K.C., Wu, A.C., Wei, C.Y., Lin, P.C., Chuang, M.C. and Yu, Y.J. (2014), "Welded end-slot connection and debonding layers for buckling-restrained braces," *Earthquake Engineering and Structural Dynamics*, **43**(12), 1785-1807.

Wu, A.C., Tsai, K.C., Yang, H.H., Huang, J.L., Li, C.H., Wang, K.J. and Khoo, H.H. (2016), "Hybrid experimental performance of a full-scale two-story buckling buckling-restrained braced RC frame," *Earthquake Engineering and Structural Dynamics*, DOI: 10.1002/eqe.2853.